Defence Research and
Development Canada

Recherche et développement
pour la défense Canada

DEFENCE **R&D** DÉFENSE

Image and processing models for satellite detection in images acquired by Space-based Surveillance-of-Space sensors

Martin P. Lévesque
DRDC Valcartier

Canada

Image and processing models for satellite detection in images acquired by Space-based Surveillance-of-Space sensors

Martin P. Lévesque
DRDC Valcartier

Defence R&D Canada – Valcartier

Principal Author

Martin P. Lévesque
Defence Scientist

Approved by

Alexandre Jouan
Section head/ Spectral and Geospatial Exploitation

Approved for release by

Christian Carrier
Chief Scientist

Abstract

In the context of the surveillance of space, known resident space objects (RSO), i.e. active satellites and space debris, need to be acquired periodically to ensure that the knowledge of their orbital parameters is up-to-date. The most sensitive observation method consists of acquiring an image sequence while the target is actively tracked by the optical system such the RSO appears stationary in the image sequence. This generates an incredible amount of data which requires efficient detection algorithms and automated processing software. In this context, this document presents models for image formation, acquisition, and processing. From the observation request to the production of the images, the stream of events is briefly modeled. This ensures that a-priori knowledge and strategy will be applied to efficiently process the acquired data. These models produce a series of algorithms used to separate the image components and detect the RSO. This document presents algorithm diagrams that can be used to develop the processing software.

Résumé

Dans le cadre de la surveillance de l'espace, les objets spatiaux connus en orbite (OSO), i.e., satellites actifs ou débris spatiaux, ont besoin d'être acquis périodiquement pour s'assurer que la connaissance de leurs paramètres orbitaux soit maintenu à jour. La méthode d'observation la plus sensible consiste à acquérir une séquence d'images lorsque la cible est poursuivie activement par le système optique et que l'OSO apparaît stationnaire dans la séquence d'images. Cela génère une quantité incroyable de données qui requièrent des algorithmes de détection efficaces et des logiciels de traitement automatisé. Dans ce contexte, ce document présente des modèles pour la formation, l'acquisition et le traitement des images. De la requête d'observation à la production des images, la chaîne des événements est modélisée brièvement. Cela permet de voir les connaissances et stratégies a priori qui peuvent être utilisées pour traiter efficacement le données acquises. Ces modèles produisent une série d'algorithmes utilisés pour séparer les composantes de l'image et détecter l'OSO. Ce document présente les diagrammes d'algorithmes qui seront utilisés pour développer le logiciel de traitement.

This page intentionally left blank.

Executive summary

Image and processing models for satellite detection in images acquired by Surveillance-of-Space Space-based sensors

Martin P. Lévesque; DRDC Valcartier TR 2009-095;
Defence R&D Canada – Valcartier; .

In Surveillance of Space (SofS), resident space objects (RSO) must be periodically observed and the measurement of their position is used to update their orbital parameters. This huge task is assumed by the Space Surveillance Network (SSN), a component of NORAD. Canada contributes to these measurements with several small telescopes. Two DND satellite projects are also in development for this purpose. They are the SAPPHIRE and NEOSSat satellites.

This document contains models that describe the image formation and acquisition process for sensors, ground-based or space-based, that acquire sequences of images of these RSO. Based on these models, it describes processing strategies, algorithms and diagrams for the automatic detection and reporting of RSOs. This document succinctly presents the lessons learned from the preceding multi-year joint (DSpaceD-DRDC) effort on satellite detection using images acquired in sidereal tracking mode. This study applies these lessons learned to detection using image sequences acquired in track rate mode (TRM). TRM is the most sensitive method and is the acquisition mode that will be implemented in the SofS satellites in development.

This study is a contribution to the data exploitation of the NEOSSat satellite. The development of models and algorithms is the starting point for the conception of data processing software. This document provides guidelines for software development. Even if the SAPPHIRE exploitation software is already in development, this document contains guidance on algorithms and processing strategies that can improve detection performance considerably. The proposed processing method may be used to upgrade the processing software for this satellite.

This processing model is designed for post-acquisition processing by ground stations where all the required computing resources are available. It is not expected the required processing capability is available on board the satellite.

Sommaire

Image and processing models for satellite detection in images acquired by Surveillance-of-Space Space-based sensors

Martin P. Lévesque; DRDC Valcartier TR 2009-095;
R & D pour la défense Canada – Valcartier .

Dans le cadre de la surveillance de l'espace (SdeE), les objets spatiaux en orbite (OSO) doivent être observés périodiquement et la mesure de leur position est utilisées pour mettre à jour leurs paramètres orbitaux. Cette tâche énorme est assumée par le 'Space Surveillance Network' (SSN), une composante de NORAD. Le Canada contribue à ces mesures grâce à plusieurs petits télescopes. Deux projets du MDN sont aussi en développement pour cette tâche. Ce sont les satellites SAPPHIRE et NEOSSat.

Ce document contient des modèles qui décrivent la formation des images et le processus d'acquisition de capteurs, basés au sol ou dans l'espace, qui acquièrent des séquences d'images de ces OSO. En se basant sur ces modèles, il décrit des stratégies de traitement, des algorithmes et des diagrammes pour la détection et la déclaration automatique des OSO. Ce document présente succinctement les leçons apprises de plusieurs années d'efforts communs (DspaceD-DRDC) sur la détection de satellites utilisant des images acquises en mode de poursuite sidérale. Cette étude applique ces leçons apprises à la détection en utilisant des séquences d'images acquises dans le mode de poursuite des satellites (TRM : track rate mode). C'est la méthode la plus sensible et c'est le mode d'acquisition qui sera implanté dans les satellites en développement.

Cette étude est une contribution à l'exploitation des données du satellite NEOSSat. Le développement des modèles et des algorithmes est le point de départ pour la conception du logiciel de traitement des données. Ce document sera utilisé comme guide pour ce développement. Même si le logiciel d'exploitation de SAPPHIRE est déjà en développement, ce document contient des algorithmes et des stratégies de traitement qui peuvent améliorer considérablement la performance de détection. La méthode de traitement proposé peut être utilisée pour une prochaine mise à niveau du logiciel de ce satellite.

Ce modèle de traitement est conçu pour le traitement différé par les stations au sol où toutes des ressources informatiques sont disponibles. On ne s'attend pas à ce que la capacité de traitement requise soit disponible à bord du satellite.

Table of contents

List of figures

List of tables

1 Introduction

To maintain a good level of space situation awareness, the orbital parameters of the Resident Space Objects (RSOs; satellites and space debris) require frequent updates. Most of the RSOs gradually deviate from their known orbits. The main causes of the deviations are the unpredictable solar activities with the resulting variable atmospheric drag, and the irregularities in the Earth's gravitational field. Thus, the RSOs require periodic observations and accurate position measurements for the recalculation of their orbital parameters. Most of these observations are done with ground-based telescopes, but space-based observation systems provide more consistent performance (no meteorological limitations, potential for 24 hour per day operation) and are becoming more available.

Because of the quantity of RSOs, all the update processes (tasking, observation and data processing) must be automated as much as possible. Usually, the degradation rate of specific orbits is known and the tasking process can be automated by selecting the TLEs older than predetermined values. A TLE, which means '*Two Lines Element set*', is a database table format that contains the orbital parameters. Then a scheduling program transforms these task requests into a series of observation requests where the selected sensors should have the optimal conditions (time, distance of RSO, phase angle, etc.) to perform their observations. The sensors are programmed and automatically perform their observations, acquiring an incredible amount of data. These data are then processed with satellite detection algorithms and the detections are reported. Finally, the TLEs are recalculated and the database updated based on detection data. This overall process, which required considerable human effort, can now be almost completely automated. It requires only minimal human intervention for system maintenance and system data integrity verification and validation.

This document addresses the automatic processing issue. In previous work (Refs 1 and 2), algorithms were developed for the detection of satellite streaks in astronomical images. These algorithms are adapted for images acquired by ground telescopes operating in sidereal tracking mode. This document considers the processing of images acquired: 1) in satellite tracking mode; and 2) by a moving space-based sensor. It describes an image acquisition model, which leads to the following processing approach and supports its development.

The goal of this document is to provide the physical and mathematical models and guidelines required for the development of future processing software that will be used with the coming space-based surveillance-of-space systems. The software is not yet developed but most of the algorithms developed for the ground-based telescope are reusable. So, there is no risky black box in the following mathematical demonstration. The fuzzy function boxes like the 'streak detector' or 'star identification' make reference to available (and already tested) commercial software or algorithms already developed and tested in previous works.

The work presented in this document begins with the development of acquisition and image formation models. This allows seeing the a-priori knowledge that can be used by the processing algorithms. Then, the image model is formulated, indicating the image components that can be separated out. The following algorithm development systematically extracts each one of these components, until it is able to isolate and report the RSO signal. Finally, the processing scheme indicates how the algorithms are linked together along with their dependencies, which provides a clear view of the global processing methodology.

This work was performed between October 2008 and May 2009 under the work breakdown element 15ee03: 'Small Telescope for the Surveillance of Space'.

2 Tasking and acquisition

Once a target has been designated for an acquisition task, programs are executed to determine when and where the observation conditions (mostly based on the brightest conditions) will be best. The 'Two Lines Element set' (TLE), which contain the orbital parameters, are the input data for a program called 'the propagator', which calculates orbits and predicts the satellite position 'R^P' and motion at the required time of observation. This operation produces a table where the sidereal coordinates '(Ra, Dec, t)', i.e., right ascension, declination, are listed as a function of the time. Note that this table is generated for specific observer's positions which are known at every moment by the propagator; this observer may be another moving satellite. The 'propagator' function is usually assumed by COTS (commercial off the shelf) software like 'Satellite Tool Kit' or 'TheSky'.

At the moment of the acquisition, these (Ra, Dec, t) coordinates are used to generate system control commands. At the appropriate moment, the optical system is pointed at the expected RSO position and the tracking rate is adjusted to maintain it in the FOV. At the appropriate time, the camera acquires the images. Because the pointing system never points exactly at the designated position (but with an acceptable error), the measured pointing parameters (Ra, Dec, Rotation and t) are recorded in the pointing data file or in image header.

Hence, at the end of the acquisition process, the available data are: the image sequence, the table of expected satellite positions and the measured pointing parameters. In addition, the image processing scheme can use a star catalogue for telemetry evaluation (astrometry) and the knowledge of the acquisition system (field of view, PSF width, etc.). This tasking and acquisition process is illustrated in Fig. 1.

TLE database

Selection of
obsolete TLE

Propagator

Expected
satellite
positions
$\mathbf{R}^P(TLE, t_k)$

Tasking

Clock: t_k

Acquisition
system

Satellite control:
pointing and
acquisition

Data

$I^0_k(t_k)$:
Image sequence

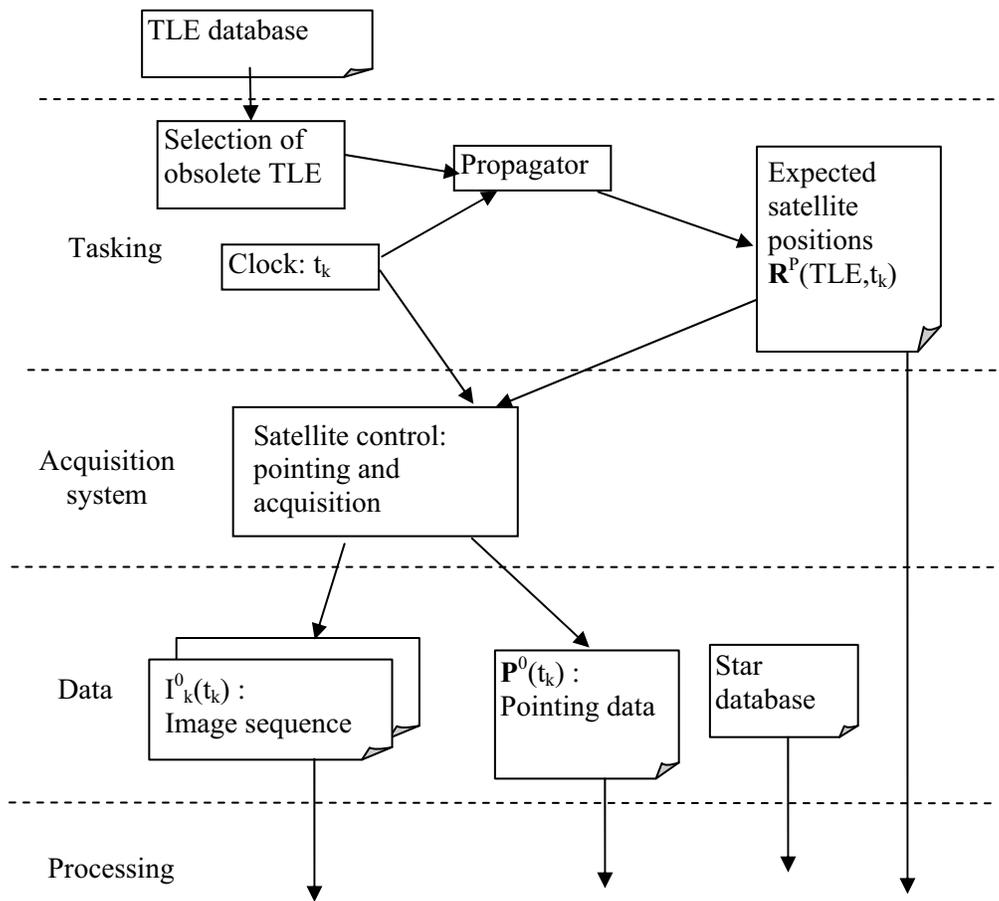$\mathbf{P}^0(t_k)$:
Pointing data

Star
database

Processing

Figure 1 – Tasking and acquisition sequence showing the a priori knowledge and the generated data

3   Scenario of image acquisition

The RSO can be acquired in two different modes; Sidereal Stare Mode (SSM) or Track Rate Mode (TRM). The sidereal mode is good for astrometry measurement and calibration but a satellite may be quickly passing out of the field of view; this makes the acquisition of a long image sequence or long exposure time impossible. TRM offers several advantages. First, the satellite brightness is concentrated within a few pixels, which increases the signal-to-noise ratio. Second, the satellite remains almost at the same image location, and several images can be acquired over longer period. Third, the satellite becomes the only static object in the image sequence, which makes it easy to detect against the moving background of stars. This also makes it easy to discriminate the flashes caused by cosmic-ray hits (CRs). However, the astrometric calibration may be less accurate. The star streaks must be detected and their centroids calculated. The accuracy of the centroids calculation is limited by the SNR, which is lower than the star SNR in SSM.

The acquisition of images in TRM mode is more complex than in SSM mode. After pointing at the appropriate location at the appropriate time, the sensor motion must be adjusted in such a way that the residual motion rate produces the expected tracking. While tracking, the sensor can acquire several images, which will produce more accurate and reliable measurements in comparison with the acquisition of a single snap shot. Furthermore, the TLE update process requires a minimum of three independent observations; this is a Space Surveillance Network 'SSN' requirement. Considering this, here is one of the most probable acquisition scenarios:

- slew/settle to a "staging" point near where the "tracking slew" is to begin,
- at the appropriate time, when the satellite enters the field of view,
   accelerate & settle in tracking rate,
- 3s exposure (first image),
- wait a few seconds before next exposure while downloading this image,
- 3s exposure (second image),
- wait a few seconds while downloading,
- 3s exposure (third image),
- wait a few seconds,
- 3s exposure (fourth image),
- slew to the next satellite position.

A minimum of four images should be acquired. A higher number would increase the system's sensitivity and accuracy. For satellites known to be bright enough, three images would be adequate (to provide the three required observations) but a fourth one is required because, quite often, a coincidental event forces the rejection of one of the acquired frame. This is the case when the RSO is overlapped by a star streak or a cosmic-ray hit. For fainter RSOs, it would be preferable to acquire a longer sequence (9 to 16 images) with a longer exposure times. This increases the SNR (signal to noise ratio – by processing with an image summation algorithm) and makes detection easier.

With a space-based system, jitter has a certain impact on image quality. It is expected that the jitter is of the same order as the size of the optical PSF. In fact, the detection algorithms must consider an effective PSF, which is the combination of the optical PSF and jitter. However, there is no intent to try to separate the jitter effect from the optical PSF, and it is not believed that it is

possible. However, there is a possibility that the jitter is not constant over the image sequence, and that some images within the sequence have a better effective PSF than others. In such a case it would be interesting to evaluate the image quality and reject the images that are more affected by jitter. However, this effect is not considered in the following algorithm development. If the usage of a space-based platform proves that jitter variations are not negligible and should be taken into account, the sensor should acquire a few extra images in expectation that not all images in the sequence will be used for detection.

The drift is also a common source of error that occurs during acquisition. It is caused by a tracking rate that does not exactly mimic the desired satellite motion. It can be taken into account by image processing algorithms. First, it distorts the shape of the PSF. This effect could be corrected with 'sharp' or 'super-resolution' algorithms, but this is not necessary for detection purposes. Second, it makes the satellite to appear at different places in the various images of the sequence. This effect is more important and is taken into account in the processing methodology presented in the document. Its correction makes it possible to apply a more sensitive global detection algorithm.

4   Scene and acquisition models

It is easy to conceive of ad-hoc processing for the acquired image. However, this processing is rarely optimal. To support a good processing approach, a good comprehension of the image formation process and scene content is necessary. This chapter presents the image model used for the image processing algorithm development. However, before arriving at an appropriate image model, it is also necessary to model the scene and other objects that contribute to form the image content.

The image content has several independent components that can be processed separately. They are the astronomical scene, RSO element (which has a different motion), cosmic-ray hits, background illumination and sensor artefacts (noise and bias). The complete image model is presented in Section 5.1. This model may seem complex, but if we look at the individual components first, then the resulting model will seem more intuitive.

4.1   Astronomical scene model

The astronomical scene content 'A' depends on the telescope field of view 'FOV', camera rotation 'Rot(t)' and the real pointing '$P^A(t)$' at the time t_k:

$$A_k(Ra, Dec) = Sky (FOV, \mathbf{P}_A(t_k), Rot(t_k)) , \tag{1}$$

i.e. A_k is a subset of the global scene 'Sky'. This expression represents a star field acquired by the camera. It can also be the result of an image reconstruction using a star database (useful for the star recognition process) or an image reconstruction resulting from the processing of the raw images.

If the pointing system is moving and the image is acquired over the time period 'dt', the resulting scene is the cumulative integration of the signal over this period of time, i.e. the interval: '$|t_k,t_k+dt$';

$$A_k (Ra, Dec |t_k,t_k+dt) = Sky (FOV, \mathbf{P}_A(t_k), Rot(t_k), |t_k,t_k+dt) \tag{2}$$

The static scene can be seen as the sum of all individual stars contained in the FOV:

$$A(Ra, Dec) = \Sigma a_n(Ra,Dec)_n , \tag{3}$$

where the individual star 'n' has their own intensity 'a_n' and position '$(Ra,Dec)_n$'. For a dynamic scene, i.e., when the telescope pointing is changing because of the tracking motion, jitter or drift, the motion blur must be taken into account:

$$A(Ra, Dec) = \Sigma a_n(Ra,Dec)_n \otimes Z(\mathbf{P}^A(t)|t,t+dt), \tag{4}$$

where '$\otimes$' is the convolution operator and '$Z(\mathbf{P}^A(t)|t,t+dt)$' is the line segment (or other streak shape) introduced by the pointing motion $\mathbf{P}^A(t)$ during the interval from t to t+dt.

4.2   Image formation and transformation

Between the sidereal scene and the image frame, the signal undergoes several transformations:

Global scene (RA,Dec),

$\rightarrow$Selected scene (RA,Dec),

$\rightarrow$ Scene sampling (i",j"),

$\rightarrow$ Optical distortion (i',j'),

$\rightarrow$ Other optical effect (i,j): final image.

One may note that the optical distortion comes before the scene sampling and this is true. But these operations are independent and their order can be swapped. The advantage of this swapped model is that the geometric distortion is now a function of the image coordinates. Otherwise, the geometric distortion should be expresses in local (Ra,Dec) coordinates and this would make the representation more complicate because (Ra,Dec) are not specific to the image. Pointing and FOV must be taken into account. When already in pixel coordinates, the geometric distortion can be easily corrected with a pixel interpolation algorithm that uses a calibrated distortion map (which is measured in laboratory). In this case, the scene sampling only means the conversion of pixel index into real space coordinates. Similarly, the other optical effect (like the PSF) occurs in the optics before the sampling by the CCD. But these effects are also independent and can be modeled on the image pixel coordinate system.

Accordingly to this model, when the telescope points in a direction $\mathbf{P}^A(t_k)$, it selects a portion of the sky 'A_k' which is delimited by the FOV and camera rotation 'Rot(t_k)'. This selects the scene:

$$A_k(\text{Ra, Dec}) = \text{Sky (FOV}, \mathbf{P}^A(t_k), \text{Rot}(t_k)) \tag{1}$$

This scene contains celestial objects whose brightness is expressed in magnitude or radiance (W/m^2/sr). For practical reasons, it is useful to think in terms of an equivalent signal expressed in pixel counts (or digital number: DN). Hence, the intensity transformation '$\mathfrak{M}$' is a function that takes into account the optical gain (aperture), sensor sensitivity and spectral match (between the object and the sensor) and produces such numbers.

$$I^A_k(\text{Ra, Dec}) = \mathfrak{M} (A_k (\text{Ra, Dec})) \tag{5}$$

The optical system creates an imperfect image of this scene, and the image formation process can be conceived in three distinct steps: the transformation '@' of the celestial scene into a perfect image grid, the transformation 'Ω' of this perfect image grid into a distorted image, and finally the addition of the optical aberrations 'Θ' like PSF. Hence, the first step of the image formation is the transformation of (Ra,Dec) coordinates into a series of temporary (i",j") indices;

$$I^A_k (\text{i",j"}) = @ (I^A_k(\text{Ra, Dec}), \tag{6}$$

where the index 'k' indicates that this transformation is specific to the image frame 'k' which was acquired at time 't_k'. This transformation links every image pixel to corresponding real sky coordinates (Ra,Dec). This image also suffers the geometric distortion 'Ω' caused by imperfect optics and the resulting image is:

$$I^A_k (i',j') = \Omega (I^A_k (i'',j'')). \tag{7}$$

Finally, the other optical effects (noise, PSF, gain, etc.) are added within the final transformation:

$$I^A_k (i,j) = \Theta (I^A_k (i',j')), \tag{8}$$

This transformation does not affect the object location like the geometric distortion 'Ω' and the transformation '$@_k$' of the sidereal coordinates into image indices. It instead reduces image "sharpness".

So, the global transformation is:

$$I^A_k (i,j) = \Theta (\Omega (@ (\mathscr{M} (A_k(Ra, Dec))))), \tag{9}$$

These transformations are reversible. Without considering the blur (caused by the PSF), the pixel coordinates are linked to sidereal coordinates with:

$$I^A_k(Ra, Dec) = @^{-1} \Omega^{-1} (I^A_k (i,j)). \tag{10}$$

To these transformations, one can add the radiometric transformation '$\mathscr{M}$' that converts the object's brightness (initially expressed in magnitude) into pixel count, but this transformation is not required in this document because all image processing algorithms only use the pixel count notation. Let us consider that this brightness to pixel-count transformation function is integrated somewhere within the optical function 'Θ'.

4.3 Astronomical calibration of an image

There are several commercial software packages like 'CCDSoft' or 'PinPoint' (Refs, 5 and 6) that can detect stars within an image, compare with a star database and evaluate image features. For example:

Software:	'PinPoint'
Input:	corrected image = $\Omega^{-1}(I^A)$
Outputs:	FOV, $\mathbf{P}^A(t)$, Rot(t) and transformation method $@_k$.

For practical reasons, let us call this operation the function 'Astrometry':

$$[@_k, FOV, \mathbf{P}^A(t), Rot(t)] \leftarrow Astrometry (\Omega^{-1}(I^A_k)). \tag{11}$$

This notation will be used later. For an accurate evaluation of the astrometric measurements, note that the image must be previously rectified (to remove geometric distortions).

4.4   Object position model

Accordingly to the TLE and prediction model, the predicted apparent position of the observed RSO (designated by 'R') is the vector:

$$\mathbf{R}^P(\text{TLE,t}) = (\text{Ra(t), Dec(t) })_R{}^P \; , \tag{12}$$

where '$\mathbf{R}^P$' is the vector and '$(\text{Ra, Dec, t})_R{}^P$' the elements of this vector. However, because of orbit perturbations, the real RSO position is:

$$\mathbf{R}^A(t) \; = (\text{Ra(t), Dec(t) })_R{}^A. \tag{13}$$

The uppercase index '^{P}' means 'predicted' and '^{A}' means an observation astrometrically calibrated. The 'Ra' and 'Dec' coordinates of the RSO are expressed as a function of time because the object and sensor are moving.

Figure 2 shows an example where the real position is not exactly the predicted one. It also indicates that the sensor is not able to point exactly at the desired position, because of limited maneuvering capabilities. In addition, the sensor does not point exactly at what is believed, because of limited sensor accuracy.

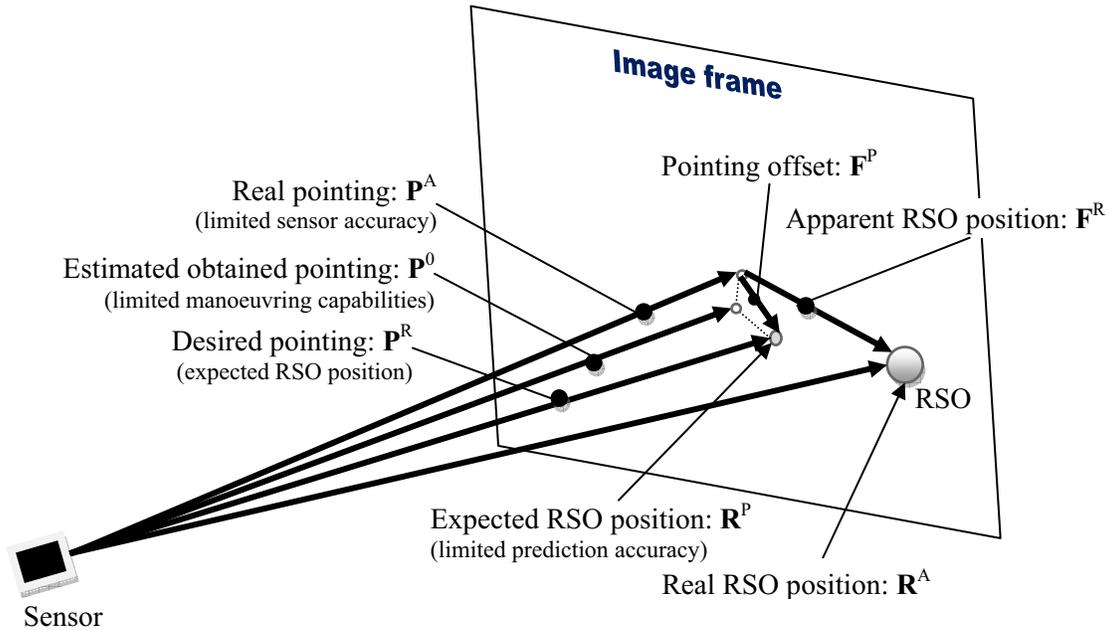*Figure 2: Estimated and real object positions and pointing vectors*

4.5   Object image model

Similarly to the astronomical content, the RSO can be projected to the image plane with transformation functions 'Ω' and '$@$' and becomes the image component 'I^R'. Its absolute position is '$\mathbf{R}^A(t_k)$' while its apparent position in the image is relative to the telescope pointing,

i.e.; $\mathbf{F}^R(t) = \mathbf{R}^A(t) - \mathbf{P}^A(t)$. It also has an intensity 'a_R', which generates an equivalent signal upon the image frame. The astrometric conversion function $@_k$ converts the RSO sidereal coordinates directly into pixel indices. If the relative position '$\mathbf{F}^R$' is used, then the pointing value must be included in the conversion.

$$I^R(t_k) = \mathcal{M}(a_R) \; \Theta \; \Omega \; @_k \; (\; \mathbf{R}^A(t_k) \;) \tag{14A}$$

or:

$$I^R(t_k) = \mathcal{M}(a_R) \; \Theta \; \Omega \; @_k \; [(\mathbf{R}^A(t_k)) \;) \otimes Z(t_k,t_k+dt) \;] \tag{14B}$$

'a_R' is the RSO magnitude while '$\mathcal{M}(a_R)$' is its equivalent in pixel counts. The function '$Z(t_k,t_k+dt)$' represents the shape of the RSO streak caused by its apparent motion. In tracking mode, it is assumed to be Dirac's delta because '$\mathbf{P}^A$' is supposed to be equal to '$\mathbf{R}^A$'. In sidereal mode this shape depends only on '$d/dt \; \mathbf{R}^A(t_k)$' and should be a line segment. However, the jitter and drift may make this function more complex. Its exact representation is:

$$Z(t_k,t_k+dt) = \; d/dt \; [\mathbf{R}^A(t_k)-\mathbf{P}^A(t)] \; dt \; = t \; d/dt \; \mathbf{F}^R(t) \; dt \tag{15}$$

4.6   Pointing model

Theoretically, the telescope should be maneuvered to point at the RSO at its predicted position, i.e. the expected pointing is:

$$\mathbf{P}^R(t_k) = \mathbf{R}^P(TLE,t_k) = (Ra(t_k), Dec(t_k) \;)_R^P. \tag{16}$$

In practice, the pointing system has some inaccuracies but can achieve a adequate pointing to ensure that the expected RSO is close to the optical axis. Using the attitude measurement systems (magnetometers, accelerometers, star tracker, etc.), the real pointing 'P^0' parameters are measured and recorded:

$$\mathbf{P}^0(t_k) = (Ra(t_k), Dec(t_k))_{P0} \approx (Ra(t_k), Dec(t_k) \;)_R^P \tag{17}$$

This pointing is only an estimation and can have a relatively large error component. The upper script '^{0}' means 'Original' pointing estimation while '^{R}' means desired pointing (at the RSO). However, after an image is acquired, the image content is checked and the known stars are identified (using comparisons with a database of reference). The real pointing parameter can be evaluated with almost the same accuracy as the star position accuracy in the catalogue.

$$\mathbf{P}^A(t_k) \; = (Ra(t_k), Dec(t_k) \;)_P^A \tag{18}$$

This pointing estimation (with the upper script '^{A}') is astrometrically calibrated and it is deduced from the image content with software like 'Pinpoint', as described previously in Eq. 11.

4.7   Tracking modes

In sidereal tracking mode, the telescope points at the object and attempts to stop its apparent sidereal motion.

$$\mathbf{P}^0(t_k) \quad = \quad (Ra, Dec)_{P0}. \tag{19}$$

In RSO tracking mode, the telescope keeps moving, trying to maintain the predicted RSO position 'R^P' in the middle of the FOV. For a short period of time, the telescope slew motion is set to constant 'Ra' and 'Dec' rates (TRM: track rate mode).

$$\mathbf{P}^0(t_k) = (Ra(t_k), Dec(t_k))_{P0} \quad \approx \quad \mathbf{R}^P(TLE,t) = (Ra(t_k), Dec(t_k))_R{}^p. \tag{20}$$

For long acquisition, active motion sensing and tracking error correction should be applied, but this is not considered in the current case where the total acquisition time is not long enough. The resulting drift is not negligible but it is taken into account and compensated in the processing described below.

4.8   Pointing offset and apparent position

The pointing offset '$\mathbf{F}^P(t)$' is error which occurs between the real pointing '$\mathbf{P}^A(t)$' (determined based upon astrometry) and the desired pointing which is the predicted RSO position '$\mathbf{R}^P(TLE,t)$'. It is obtained with the vector subtraction;

$$\mathbf{F}^P(t) = \mathbf{R}^P(TLE,t) - \mathbf{P}^A(t), \tag{21}$$

where '$\mathbf{P}^A$' and '$\mathbf{R}^P$' are unit vector but not '$\mathbf{F}^P$'.

Similarly, the apparent position of the RSO is the difference between its real position and the real telescope pointing parameters:

$$\mathbf{F}^R(t) = \mathbf{R}^A(t) - \mathbf{P}^A(t) \tag{22}$$

This is the value the data acquisition and processing will determine.

4.9   Drift estimation

Drift 'D' appears when the pointing is changing during the acquisition because of residual unpredicted pointing motion. An example is illustrated in Fig. 3. In sidereal mode, the camera should stare at the stars. The pointing should be constant from one frame to another. Usually, star trackers are used and the pointing accuracy is maintained with a dynamic feedback loop. However, in TRM, the motion is estimated and the satellite is maneuvering consequently. It is virtually impossible to verify the tracking, or at least not with an accuracy similar to that provided by star trackers. With the astrometric calibration, the real pointing position can be measured and the pointing motion can be evaluated by comparing the pointing of different frames:

$$\mathbf{D}(t) = d\mathbf{P}^A(t)/dt \; dt \; \text{ or } \; d\mathbf{P}^A(t)/dt \; t \tag{23A}$$

or

$$\mathbf{D}(t_k) = \mathbf{P}^A(t_k) - \mathbf{P}^A(t_{k-1}) \ . \tag{23B}$$

where 'k' is the image frame index and 't_k' the time of acquisition (not the exposure time) and dt the integration period (which is the exposure time 't'). This drift value '$\mathbf{D}(t_k)$' will be used later in the image processing section for the realignment of images.

In TRM, a similar drift can be estimated. It is assumed that the RSO position is only known approximately, but its motion (relative to the sensor) is known with accuracy. Thus, assuming that the camera is not rotating, the drift can be estimated by comparing the real pointing relative to the estimated RSO position (i.e. the pointing offset) in time;

$$\mathbf{D}(t) = d/dt \ \text{-}\mathbf{F}^R(t) \ \ dt \ \ = d/dt\text{-} \ \mathbf{F}^P(t) \ dt \ = \ d \ (\text{-} \ \mathbf{P}^A(t) + \mathbf{R}^P(TLE,t)) \ /dt \ \ dt \tag{24A}$$

or:

$$\mathbf{D}(t_k) = [\ \text{-}\mathbf{P}^A(t_k) + \mathbf{P}^A(t_{k-1}) + \mathbf{R}^P(TLE,t_k) \ \text{-} \ \mathbf{R}^P(TLE,t_{k-1}) \ ] \tag{24B}$$

Once the astrometric conversion '$@_k$' is known, the drift can be translated into pixel (i,j) displacement per frame, i.e.: $(di/dk,dj/dk)$. Because the optical axis is the image central pixel (i_0,j_0), this can also be thought of as corresponding to the pointing vector translated into image coordinates:

$$(i_0,j_0) = \Omega \ @_k \ (\mathbf{P}^A(t_k), \tag{25}$$

the relative displacement provided by the drift is:

$$\mathbf{D}_k = (di/dk,dj/dk) \ = \ [\ \Omega \ @_k \ (\mathbf{P}^A(t_k) + \mathbf{D}(t_k) \ ) \ ] - (i_0,j_0). \tag{26}$$

In summary, it is important to note that this drift estimation method has the ability to compensate for two important sources of error. First, for cases where the optical system can only achieve poor pointing accuracy, this does not affect the processing capability, since the drift is estimated using the astronomical image content. Second, if the RSO motion has important changes (because of the relative motion between the RSO and the observing telescope), this is automatically taken into account by propagation model (which calculates RP(TLE,t)). Hence, this set of equations facilitates evaluating the exact drift and relative displacement and makes possible exact image realignment.

4.9.1 Detecting several co-located RSOs

Usually, co-located RSOs have almost the same orbital parameters. For a short period of time, they do not have apparent relative motion. They move as a single body. Hence, the previous drift estimation will allow the detection of such a group of RSOs (common in GEO belt). However, if the apparent relative motion becomes apparent, the previous set of equation can be adapted simply by defining a position vector '$\mathbf{R}^P(TLE,t)$' for each one the expected RSO. This will be more CPU intensive but the case remains manageable.

Real pointing: $\mathbf{P}^A_3$

Real pointing: $\mathbf{P}^A_1$

Drift: $\mathbf{D}_3$

Desired pointing: $\mathbf{P}^R_k$

RSO

Expected RSO position: $\mathbf{R}^P_k$

Real RSO position: $\mathbf{R}^A_k$

Sensor

Image frame

Image sequence

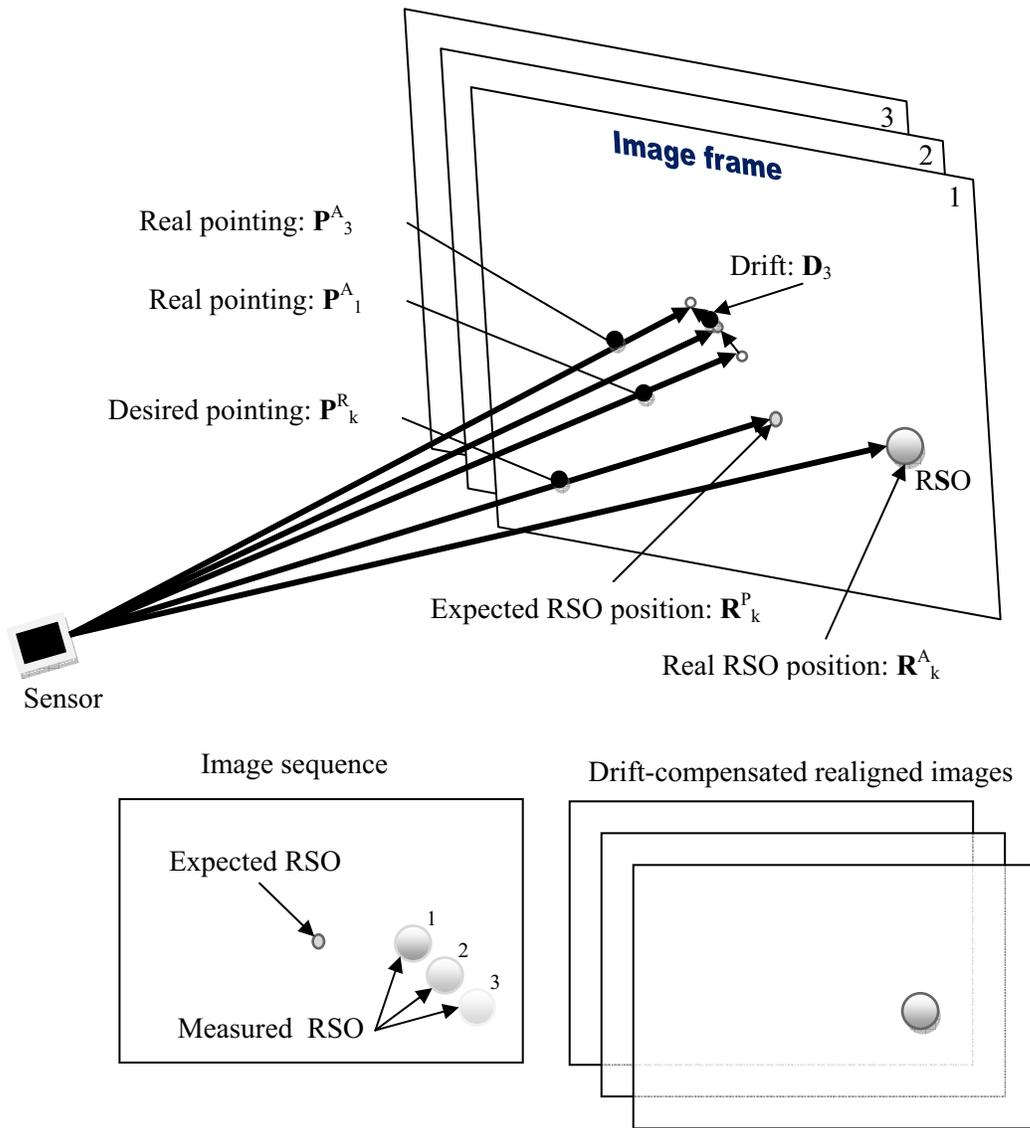Expected RSO

Measured RSO

Drift-compensated realigned images

Figure 3: Drift measurement, in tracking mode, relatively to the expected RSO positions

5 Image model and processing

The previous chapter provides us with information that can be used in image processing algorithms; the scene and RSO image components. It remains to add the none-image components to the image model: sensor noise and bias, cosmic-ray hits and diffuse light sources. With a complete model, it will be possible to establish a method for the extraction of a specific component such as the RSO, which is the goal of this study.

5.1 The image model

The image content can be described using the following model. The original image acquired by the sensor (with the superscript '0' for 'original') depends on the telescope pointing parameters '$P^A(t_k)$' at the time 't_k', the CCD temperature 'T', the exposure time 't' (which replaces the time interval dt), the FOV and other optical parameters hidden inside the optical function 'Θ'. For an image sequence, the 'k^{th}' images of the sequence, acquired at time 't_k', is:

$$I^0_k = I^0(T,t_k,t, P^A(t_k))) = I^A(t_k,t) + I^R(t_k,t) + B_k(T,t, P^A(t_k)) + n_k(T,t) + C_k(t).$$

(27)

'I^0' is the summation of the independent astronomical 'I^A' and RSO 'I^R' scenes, background 'B', noise 'n' and cosmic-ray hits 'C'. The astronomical and RSO content 'I^A' and 'I^R' images are previously defined in Eqs. 9 and 14. This image model should also include a description of hot and dead pixels. In practice, this information can be recorded on static maps and the images can be corrected in a pre-processing step.

The goal of the following image processing techniques are to separate these independent components and isolate the $I^R(t_k,t)$ component, which is necessary for achieving detection.

5.2 Background estimation and removal

The image background 'B' is principally caused by sensor artifacts '$Dk(T,t)$', and depend on temperature, exposure time and other sensor characteristics (like the dark current, DC offset, ADC noise, etc.). However, it may also contain external sources 'L_1' like zodiacal light (or diffuse nebula) or stray light 'L_2' and these components change with the telescope pointing.

$$B_k(T,t, P^A(t)) = \mathcal{D}_k(T,t) + L_1(P^A(t_k), t) + L_2(P^A(t_k), t)$$

(28)

Stray light can be produced by strong light sources close to the field of view. Particular effort is applied to stay away from the Sun, the Moon and the Earth's horizon. Very bright stars like Vega or Sirius can also produce visible stray light and significantly contribute to the background. With a very good optical design and meticulous operation, L_1 and L_2 should not be significant light components and can be ignored most of the time, but there is no guarantee they will never appear.

This background 'B_k' is harmful to the image compression or other image processing algorithms. 'B_k' must be estimated ('$<B_k>$') and removed. Good background estimation methods are

presented in Ref. 4. A 'good' estimation method is one that produces a minimal residue '$\mathcal{R}$', i.e., the difference between the real background and the estimation, is less than the noise amplitude;

$$\mathcal{R}_k = |\, B_k(T, t, P^A(t_k)) - <B_k(T, t, P^A(t_k))> | \; < \sigma_n, \tag{29}$$

There are several methods to evaluate image background '<B>' (Refs. 1 to 4). The most popular remains the measurement of the dark frame '$D_k(T,t)$' (Ref. 3) by acquiring an image with a closed shutter. However, if L_1 or L_2 is present, it is not included in this background estimation. Even if L_1 and L_2 are null, there is no guarantee that the dark frame subtraction method will leave a residue at an acceptable level. Reference 3 demonstrated that dark frames acquired with a very small temperature difference may leave a large residual dark-frame count, i.e.;

$$\mathcal{R}_k = |\, \mathcal{D}(T_k, t) - \mathcal{D}(T_k + dT, t)\,| \; > \sigma_n \;\; \text{if} \; |\, dT\,| > \text{'temperature tolerance'} \tag{30}$$

With the tested CCD (in Ref. 3), the temperature tolerance (to obtain an acceptable residue) was no more that 0.1C and this was less than the temperature measurement accuracy. This was an unsatisfactory CCD. Note that there is always a small temperature fluctuation caused by the feedback-loop hysteresis between the temperature measurement and cooler-system control. It is possible that the measured temperature be never exactly the CCD temperature (depending on the location of the temperature sensor).

A possible solution to minimize the residue is the acquisition of several dark frames (at different temperatures 'T_n') combined with a very accurate CCD temperature measurement system. The appropriate dark frame could be interpolated from these references;

$$\mathcal{D}_k(T_k, t) = \; a\, \mathcal{D}(T_1, t) + \; b\; \mathcal{D}(T_2, t), \tag{31A}$$

$$b = (T_k - T_1) / (T_2 - T_1), \text{ and} \tag{31B}$$

$$a = 1 - b. \tag{31C}$$

This method is the most economical in terms of CPU capability and may be used onboard a satellite. Usually, the same dark frame is used for an entire image sequence, but if temperature changes during the sequence acquisition, there is a possibility of adapting the dark frames for every individual image frame.

The other methods (Refs. 1 and 4) consist of evaluating the background by software which assumes that the background is a smooth function while the celestial objects are sharp and always brighter than the background. If L_1 and L_2 are present and correspond to this background characteristic, they are automatically included in the background estimation. References. 1 and 4 describe iterative methods based on polynomial fit or local statistics. These methods converge quickly toward very accurate estimations. The background residue produced by these methods is less than $0.2\,\sigma_n$. However, they are CPU intensive, and sufficient computing capacity may not be available on a satellite. However, they are adequate for deferred processing performed by ground stations.

The current case (image sequence) has another characteristic that is neither exploited by the dark frame method nor the iterative local estimation of Refs 1 and 4. This static background is systematically present in every frame of the image sequence. In TRM mode, the background is almost the same in every frame, and the stars never appear at the same place. Only the satellite

appears at the same place if it is perfectly tracked. A first background estimation can be obtained by extracting the minimum of the image sequence:

$$I^{min} = \text{minimum } (I^0_1, \ldots, I^0_K) \tag{32}$$

The drawback of this estimation is that it underestimates the background because of a negative bias introduced by the systematic selection of all negative noise peaks. It also includes all static objects like very well tracked RSO. A median filter should produce better results;

$$I^{med} = \text{smoothing } (\text{median } (I^0_1, \ldots, I^0_K)) \tag{33}$$

This estimation should ignore single bright events like the presence of star streaks or cosmic-ray hits in a single frame. A smoothing operation may be required to obtain a background without texture. Equation 31 should also provide a better background average because it does not systematically extract the minimum noise spikes. However, it will always contain static objects. So, the smooth background assumption must be used again, i.e. a static object, like a well-tracked RSO, is small (compared with the image size), relatively sharp (almost the PSF shape) and brighter than the background while the background is smooth and dark. So, the following assumptions can be made:

1) a smoothed background still represents the background,
2) a smoothed image (RSOs + Background) contains a background with a very attenuated RSOs,
3) the minimum between the background and the smoothed background remains the background, except for point objects (RSO) which are severely attenuated.

The background estimate is obtained with the function;

$$<B_k> = \text{minimum } (I^{med}, I^{med} \otimes \text{'large impulse response'}). \tag{34}$$

By repeating the process with an iterative scheme, the RSO completely disappears, leaving only the background. This method is described in detail in Ref. 4 where the background is evaluated in the presence of stars and where the stars are eliminated from the background by using this approach:

$$<B_{k1}> = I^{med}, \text{ (i.e. the first estimate)} \tag{35}$$

$$<B_{kn}> = \text{minimum } (<B_{kn-1}>, <B_{kn-1}> \otimes \text{'large impulse response'}). \tag{36}$$

Once the background is adequately estimated, a background-free image 'I^{-B}' can be produced (Ref. 1 to 4).

$$I^{-B}_k = I^0_k - <B_k> \tag{37}$$

$$I^{-B}_k = I^A_k + I^R_k + n_k + C_k + \mathcal{R}_k \tag{38}$$

and $\mathcal{R}_k \approx 0$. The upper script '$^{-B}$' means background removed.

5.3 Star detection

The next step consists of detecting the stars. This detection will have several usages. First, the detected stars are used to measure astrometry parameters, i.e., the real pointing values of the telescope $P^A(t_k)$ along with the measurement of the image rotation. Second, astrometry is used to measure the drift (in satellite tracking mode) of the telescope pointing relative to the expected satellite position. Finally, the presence of stars is a "determinate false alarm source" relative to satellite detection. The better we are able to predict and subsequently remove false alarms, the easier RSO detection will be.

Depending on the tracking mode, the stars appear like streaks or points (with a PSF profile). In Ref. 1, methods were developed for the detection of these two kinds of objects. Sidereal tracking mode is well solved in Ref. 1. Here, the effort will be focused on constant track rate mode (TRM).

In tracking mode, the stars appear in the image as streaks. They also appear fainter because their energy is spread over more pixels. Thus, the detection methods using clipped signal and Hough transform may not be appropriate when there are not enough bright stars in the FOV. In such a case, the matched filter described in Ref. 1 is more appropriate for this task. This method is able to detect a single streak as faint as ISNR=0.5, i.e., an average signal-to-noise ratio of 0.5 per pixel. However, such a sensitivity may not be required if there are enough very bright stars.

The detection method of Ref. 1 can produce: 1) an image 'I^{+S}' that contains only the star streaks, 2) the list of the centroids for each one of these streaks '$S_k(n,i,j)$', and 3) a binary image mask 'M^S_k' which locates the streak pixels in the background-free image 'I^{-B}_k'.

$$\text{Streak\_detector}(I^{-B}_k) \rightarrow [I^{+S}_k, S_k(n,i,j), M^S_k] \qquad (39)$$

The follwing describes the method explained in Ref. 1. The background-free image 'I^{-B}_k' is convolved with the expected streak shape '$Z(P^A(t_k)|t_k,+t)$'. The convolved image 'Λ_k' contains convolution peaks which indicate where the streaks are.

$$\Lambda_k = I^{-B}_k \otimes Z(P^A(t)|t,t+dt) \qquad (40)$$

The iterative convolution and clipping method of Ref. 1 allows improving filtering performance ('$_m$' is the iteration index) ;

$$\Lambda_{km} = I^{-B}_{km} \otimes Z(P^A(t)|t,t+dt), \qquad (41)$$

and

$$I^{-B}_{k(m+1)} = \text{minimum} \{I^{-B}_{km}, 2\Lambda_{km}\}. \qquad (42)$$

Once the iterative process converges toward a stable solution (about three iterations normally improves significantly the performance), the final convolved image is clipped at a predetermined threshold to produce a binary extraction mask 'M^S_k'. In the case of multiple streak detection, this threshold should be a value close to the noise level 'σ_n';

$$M^S_k = \Lambda_k > \sigma_n. \qquad (43)$$

The image 'I^{+S}_k' containing only the star streak is obtained by multiplying this mask by the background-free image:

$$I^{+S}_k = M^S_k * I^{-B}._k \qquad (44)$$

This image should contain all major astronomical objects and is a very good estimation of the astronomical scene defined in the image model, i.e.:

$$I^A(t_k,t) \approx I^{+S}_k . \qquad (45)$$

For the localization of every individual star, the mask 'M^S_k' is segmented into 'N' individual objects 'M^S_{kn}'. The segmentation method is presented in Ref. 2;

$$M^S_k = \Sigma M^S_{kn}. \qquad (46)$$

For each streak, a sub-image 'I^{+S}_{kn}' is extracted by multiplying the background-free image by the corresponding single-object mask;

$$I^{+S}_{kn} = M^S_{kn} * I^{-B}. \qquad (47)$$

The center of intensity 'i,j' (same calculation as the center of mass) and total intensity 'a_n' is calculated for every 'n' streaks and a global list '$S_k(n,i,j,a_n)$' is produced;

$$S_k(n,i,j,a_n) = [n, (i,j)=\text{center of mass } \{ I^{+S}_{kn} \}, a_n = \text{total intensity } \{ I^{+S}_{kn} \}]. \qquad (48)$$

5.4 Star streak removal

Once the star streaks are detected in the image and the mask 'M^S_k' produced, the image without stars is obtained via:

$$I^{-S}_k = I^{-B}_k (1 - M^S_k). \qquad (49)$$

The super script '-S' means the streaks are removed from the image (the annotation 'I^{-B-S}_k' could also be used). According to the image model, this image should contain only the RSO plus the noise and cosmic-ray hits;

$$I^{-S}_k \approx I^R(t_k,t) + n_k(T,t) + C_k(t). \qquad (50)$$

However, Eq. 47 may leave signal artifacts. When the streaks have extended PSF profiles and the mask is too narrow, only the middle part of the streak is erased, leaving truncated signals with halo shapes around the erased objects. With the multi-frame detection method explained in Section 5.6, these artifacts should not have serious impacts on the detection results. But if this is the case, Ref. 1 indicates a more accurate method for the removal of PSF-shaped objects that do not leave such artifacts. Removing such PSF shaped objects will require additional calculations, but it will not present a technical challenge.

The removal of the star streak should reduce the production of false alarm, later in the RSO detection phase. However, it is not sure that this is necessary; the RSO detector can be design to detect the RSO, even in presence of stars, as explained later in section 5.7. This is a question of

performance, evaluated by testing with simulated data first and then with real data, that will determine is the removal of the star streaks increase the detection reliability.

5.5 Image alignment with drift correction

After the removal of star streaks, it should be relatively easy to detect the RSO in the residual image. However, the cosmic rays produce strong artefacts, usually brighter that faint RSO. The method for discriminating between the RSO and cosmic rays consists of analyzing the entire image sequence. In tracking mode, the RSOs should systematically appear at the same place while the cosmic-ray hits appear at random places. The RSO steady-state condition is respected only in the absence of drift or with compensated drift. Thus, in the presence of a drift, the image sequence needs to be realigned before comparing the pixels.

With the previously defined drift (the difference between the real pointing $P^A(t)$ and the RSO expected position $R^P(TLE,t)$), i.e.:

$$\mathbf{D}_k = (di/dk, dj/dk) \; = \; [\; \Omega \, @_k \, (\mathbf{P}^A(t_k) + \mathbf{D}(t_k)) \;]\; - (i_0, j_0). \tag{26}$$

it is possible to calculate the cumulative drift 'X' (from first to last frame) and realign the image sequence frames relative to the first frame (the 'X' mnemonic is used due to running out of letters in the alphabet, sorry for this bad mnemonic):

$$X_k = (X_{ik}, X_{jk}) = \sum_1^k \mathbf{D}_k \, , \text{ where } 1 \le k \le K, \tag{51}$$

where 'K' is the total number of images in the sequence.

The image frame 'I^{-S}_k' can be realigned by shifting the image by an equivalent cumulative drift displacement;

$$I^{-D}_k = I^{-S}_k \,(i - X_{ik}, \, j - X_{jk}). \tag{52}$$

Hence, all the realigned images of the sequence 'I^{-D}_k' should present the RSO at the same pixel location. To make a long story short, the upper case '$^{-D}$' means the drift is now removed or compensated. For the complete story, one should write: 'I^{-B-S-D}_k' because the background and stars were also previously removed, but this would only produce a more confusing notation.

The interest of the image alignment is that all the image frames can be summed to produce a single image 'I^Σ' where the RSO's SNR is improved by a factor '$\sqrt{K}$'. This assumes a Gaussian noise, which is very close to reality.

$$I^\Sigma = \sum_{k=1}^K \; I^{-D}_k \tag{53}$$

According to the image model of Eq. 27, which is reduced to Eq. 50 after the removal of background and stars, the sum of the realigned images is:

$$I^{\Sigma} \approx \sum_{k=1}^{K} \ [\ I^R(t_k,t) + n_k(T,t) \ + \ C_k(t) \ ] \ . \tag{54}$$

$$\approx \ K \ I^R(t_k,t) + n_\Sigma \ (T,t) \ + \ \sum_{k=1}^{K} \ C_k(t). \tag{55}$$

Using the noise addition rule where $\sigma_\Sigma^2 = \sqrt{(\sigma_1^2 + \sigma_2^2)}$; $\sigma_{n\Sigma} \approx \sqrt{k} \ \sigma_{nk}$. The signal amplitude increases with the number of sample images 'k', while the noise amplitude only increases with the $\sqrt{k}$ rule. For example, with an original RSO SNR = 4, which is very border-line for the detection, the new SNR is improved to '12' for a sequence of nine images, which results in a more readily detected RSO.

5.6   Detection of the RSO

With this last image, the challenge is the detection of a signal above the noise level with the rejection of the often brighter cosmic-ray hits.   Let us consider the following signal characteristics:

- The RSO is almost constant in every image. Only the possible detections are considered, i.e., RSO brighter than the noise level.
- Cosmic-ray hits can be very bright but appear in the image sequence at random.

Hence, the first detection is perfomed using the summed image with a high detection threshold 'h_h':

$$\Delta_{ij} = \ I^{\Sigma}(i,j) \ \geq h_h \ . \tag{56}$$

'Δ' is a binary alarm matrix. Typically, h_h is greater than 2 to 3 times the noise level, which is $\sqrt{K}\sigma_n$ in the summed image. So, a typical h_h is:

$$h_h = \ 3\sqrt{K}\sigma_n \tag{57}$$

After the detection with the summed image, the detected object can be track back in individual image frames and detected again with a lower detection threshold value 'h_l', which is applied only within the region of interest identified by the global detection. Hence, for a global detection 'Δ_{ij}', there is a series of individual local detections 'Δ_{ijk}'. Hence, the complete detection test is:

$$\Delta_{ij} = \ [\ I^{\Sigma}(i,j) \ \geq h_h \ ] \ \text{ and } [\ \prod_{k=1}^{K} \ (I^{-D}{}_k(i,j) \ \geq h_l) \ ], \tag{58}$$

where 'Π' is the product of all logical conditions, i.e. equivalent to a 'AND' logical operator.

For a sequence of nine images, the 'h_h' could be $9\sigma_n$ while 'h_l' could be as low as $2\sigma_n$ (even $1\sigma_n$ should be tested). The exact threshold value will have to be fine tuned with real data and false alarm tolerance constraints.   However, $9\sigma_n$ and $2\sigma_n$ are good assumptions and they will be considered as values of reference.

The limit of sensitivity of this filter is SNR>3 (when 9 images are summed, the integrated SNR triples and pass the test of Eq. 58). It can reject cosmic-ray hits of any intensity. Table I indicates

the behaviour of the combined tests. To detect a RSO, the global and all individual tests must succeed. The very faint (SNR>3) RSO will pass the global test and all tests in the individual frame. Once in a while, the noise will succeed the detection test in a frame (and generate a false alarm) but never the global test in the summed image. A cosmic-ray hit may be so intense that it may succeed the global test, but in the second test, most of the individual frames (which contain only noise) will fail. Perhaps, once in a while, a combination of noise and background residue will pass the tests. In such a case, the background residue probably cover an extended area and the non-PSF shape can be used to reject similar cases.

One may be tempted to use only the second test, but the combination of both tests makes detection more reliable and more sensitive. The noise and background residue can create false alarms with the second test but will never trigger the first one. With a higher threshold value 'h_l' (which would reduce the false alarm rate), the combination of the faint RSO signal and noise may fail the second test. This would make the system less sensitive and this is not desired. Therefore, the combination of both tests assures sensitivity and false alarm rejection.

5.7   Detection of a RSO in presence of a star streak

It is possible that the RSO overlaps a star streak in one (or more) of the frames. If this occurs, this RSO signal should be erased with the streak with the consequence that the detection with Eq. 58 fails. This situation can be corrected by inclusion of the star streak mask within the detection algorithm. First, the streak mask 'M^S_k' must be aligned with the realigned image:

$$M^{S\text{-}D}_k = M^S_k (i\text{-} X_{ik}, j\text{-}X_{jk}). \tag{59}$$

With this modified detection rule;

$$\Delta_{ij} = [\ I^\Sigma(i,j) \geq h_h\ ] \ \text{and} \ [\ \prod_{k=1}^{K} \{\ (I^{\text{-}D}_k(i,j) \geq h_l)\ \} \ \text{or} \ \{\ M^{S\text{-}D}_k(i,j) = 1\ \}\ ], \tag{60}$$

The erased RSO (erasure due to a star streak mask) will not invalidate the detection. However, when this situation occurs, it must be reported and the concerned frames (where star streak or streaks overlap the RSO) must not be considered for the RSO brightness estimation. Concretely, if there are 9 images used for RSO detection, and in two of the nine images star streaks overlap the RSO, only the seven other images (non star-streak/RSO overlap images) are used in the RSO brightness calculations.

	$I^\Sigma(i,j) \geq 9\sigma_n$ Does the global test succeed?	$I^{-D}(i,j) \geq 2\sigma_n$ Do the individual tests succeed?	$\displaystyle\prod_{k=1}^{K} (I^{-D}(i,j) \geq 2\sigma_n)$ Do the K individual tests succeed?
RSO + noise SNR=4 in individual frame, SNR=12 with the summation of 9 frames.	**Always**	**Always**	**Always**
Noise only	**Never**	**Sometimes**; noise events above $2\sigma_n$ (3% of pixels).	**Never**
Cosmic-ray hit + noise	**Often**; bright flash	**Sometimes**: the frame that contains the cosmic-ray hit and noise events above $2\sigma_n$.	**Never**
Noise with background residue	**Never**	**Sometimes**; noise events + background residue above $2\sigma_n$	**Possible**

Table I:
Result of the tests for an RSO with a SNR=4 and a sequence of 9 images

5.8   Detection of a RSO with a corruption by a CR

A CR will not prevent the detection of an RSO. However, it will corrupt the calculation of the RSO centroid in the frame where it appears. Thus, the Cosmic Ray noise artefact must be detected and the corrupted centroid must be ignored. When an RSO is detected with the previous tests, the intensity regularity can be verified. For a detection 'Δ_{ij}' at coordinates (i,j), the expected RSO intensity '$<I^{RSO}>$' is well estimated with the median filter (applied on the drift compensated images):

$$\text{For } \Delta_{ij}=1: \quad <I^{RSO}(i,j)> = I^{-D\ med}(i,j) = \text{median } (I^{-D}_1(i,j), I^{-D}_2(i,j)\dots, I^{-D}_K(i,j)). \tag{61}$$

The accepted brightness increment, for a specific observation 'k', should be less than a predefined tolerance 'h_t';

$$I^{-D}_k(i,j) - <I^{RSO}(i,j)> \quad < h_t . \tag{62}$$

The variation tolerance should be something close to $2\sigma_n$ (maybe $3 \sigma_n$) for faint RSO or a fraction of the brightness for brighter RSO. Only the photon and sensor noises should be responsible for the variation, perhaps including the PSF influence and possibly a certain tolerance to the jitter. 'h_t' could be defined with an ad-hoc function similar to:

$$h_t = 3 \text{ sqrt } (\sigma_n^2 + c <I^{RSO}(i,j)>), \tag{63}$$

which considers the sensor noise and Poisson nature of the signal. This assures a minimum tolerance that depends on the noise level. This tolerance increases with stronger RSO signals (where variations will be greater). The function takes into account the Poisson-distribution nature of the photonic signal. The constant 'c' represents the ratio of photon-to-DN (digital number) conversion. One kind of error that Eq. 63 does not take into account is the signal quantization or 'pixelization'.

If one of the RSO measurements is much brighter than the predefined tolerance for an individual image, then a cosmic-ray hit can be suspected. Recall that the star streaks have already been erased and that the test of Eq. 62 does not take intensity decrement into account. Thus, when the product of all intensity tests succeeds and the brightness is very constant, then an uncorrupted RSO detection can be declared with;

$$1 = \prod_{k=1}^{K} [\{ | I^D_k(i,j) - <I^{RSO}(i,j)> \} \quad < h_t] \quad ; \text{constant brightness} \tag{64}$$

Else, when one of the 'k' tests fails, it multiplies the result by zero. This means that a pixel is much brighter than the tolerated variation. This is an indication of a corruption by a cosmic-ray hit. In that case the measurement must be ignored in the evaluation of the RSO position.

Note that this test does not work with a fast tumbling satellite – that implies significant brightness variation over time. However, the tumbling is supposed to be an a priori knowledge when a satellite acquisition is tasked. Thus when such a case is present, it will require different detection conditions and potentially algorithmic customizations to account for significant variations in RSO signal strength during the RSO imaging sequence.

5.9 Refinements of detection algorithms for the improvement of performance and stability

It is possible to improve the detection performance with a few ad-hoc modifications. These modifications take into account that 1) processing artefacts can be attenuated, 2) the signal is not completely exploited and 3) evaluation errors can be corrected or compensated. Here are a few examples.

5.9.1 Elimination of the background residue

When the background is estimated with the iterative method of Eq. 36, it is expected that it leaves a residue '$\mathcal{R}_k$' that is almost null. However, when the image sequence is summed into a single image containing the total signal (Eq. 53), the sum of the residues may create a significant signal. Hence, Eq. 36 can be applied again on the image of total signal 'I^Σ', evaluating the global residue, which creates a new background. It is not expected to be more than a fraction of the noise level multiplied by the number of image frames. This value is small but probably measurable and it can affect the detection tests. This new global background can be subtracted, reducing the total residue and improving the detection condition of Eq. 54.

$$<B_\Sigma> = I^\Sigma \otimes \text{ 'large impulse response'}. \tag{65}$$

$$I^{\Sigma'} = I^\Sigma - <B_\Sigma> \tag{66}$$

A more sophisticate method could consider recalculating the image summation with exclusion of signal above the noise level.

5.9.2 Integration over the PSF area

The previous algorithms do not take into account that the signal can be degraded by the PSF. Detection sensitivity can be increased by integrating the signal over the effective PSF area. This can be achieved simply by using local summation. According to Annex B of Ref. 2, the SNR is optimal when the summed area matches the PSF area. For example, when the PSF width is 3 pixels at the half height, a summation over an area of 3x3 pixels can be used. This can effectively double the SNR. Here, the 'square root' rule cannot be used because the pixels do not all have the same weight. This number (double SNR for a 3x3 window) was obtained by integrating a Gaussian PSF profile (3-pixel width at half height) in the presence of Gaussian noise.

For a detection with integrated area, one has only to replace the images 'I^Σ' and 'I^{-D}_k' in Eq. 58 by their equivalent locally summed images like (here for a PSF width equal to 2n+1 pixels);

$$I^{-D\ PSF}_k(i,j) = \sum_{i-n}^{i+n} \sum_{j-n}^{j+n} I^{-D}_k(i,j) \tag{67A}$$

$$I^{\Sigma\ PSF}(i,j) = \sum_{i-n}^{i+n} \sum_{j-n}^{j+n} I^\Sigma(i,j) \tag{67B}$$

5.9.3 Increase the tolerance to drift estimation errors

The detection algorithms also consider that the images are perfectly realigned. This may not be the case. The astrometric calibration of the celestial pointing vector '$\mathbf{P}^A$' may leave an error of one or two pixels in the drift estimation. The RSO may not be perfectly realigned in the corrected image sequence.

The detection condition of Eq. 58 can also be slightly modified to accommodate a certain level of error in the image alignment. Rather than comparing aligned pixels, it may be better to compare local maxima. The detection algorithm could accept a situation like this one: a target succeeds the tests in the successive frames at the locations: $(i,j)_1$, $(i.j+1)_2$, $(i-1,j)_3$, etc., with more or less one pixel of jitter from frame to frame. With appropriate threshold values (and background correctly removed) there is almost no chance that noise pattern succeeds in generating a false alarm, even though this probability increases. A simple method can be implemented to increase position error tolerance; simply replace images 'I^{-D}_k' by one of local maxima such as;

$$I^{-D\ max}_k(i,j) = \max (I^{-D}_k(i-n:i+n,j-n:j+n), \tag{68}$$

where 'n' is the tolerated displacement and 'i-n:i+n' the index sequence 'i-n, …, , i, …, i+n' (like the Matlab notation). This algorithm modification can be chained in cascade with Eq. 67.

5.10 Calculation of RSO centroid

Once the detections are known, the exact position of the RSO must be determined. This calculation is done with all the pixels that may contain signal, even those that do not contribute to the detection but surround the detected pixels. Thus, a small sub-image 'I^{-D}_{kn}', centered on the detected pixel 'Δ_{ij}' and larger than the PSF, is extracted;

$$I^{-D}_{kn} = \text{extract\_kernel} (I^{-D}_{k}, \Delta_{ij.n}) \tag{69}$$

The 'extract_kernel' is a function that selects a group of pixels centered on the nth detection at location (i,j) with a width determined by the PSF width. The center of intensity (same calculation as the center of mass) is calculated with a sub-pixel accuracy and this location is reported in the frame of reference of the image 'I^{-D}_{k}'. Before the calculation of sidereal coordinates the drift value 'X_k', which was removed by the image realignment, must be re-introduced into the final position;

$$\mathbf{R}^{A}_{kn} = (i,j)_R A = \mathbf{X}_k + \text{center of intensity } (I^{-D}_{kn}). \tag{70}$$

So the astrometric conversion, known for this frame, can be applied.

$$\mathbf{R}_{kn}{}^{A}(t_k) = @_k^{-1} (\Omega^{-1}(\mathbf{R}^{A}_{kn})) \tag{71}$$

5.11 Cleaning flashes caused by cosmic-ray hits

In some cases, it might be interesting to remove the cosmic-ray hits from the images, even though this was not necessary for the detection. In fact, it is usually believed that the cosmic-ray hits must be erased first. The acquisition of an image sequence is normally done for this purpose and a 'voting' filter eliminates the bright pixels that appear in only one frame. If this is done first, this would also erase the star streaks (which appears at different places in time) and make astrometry calibration difficult. This would also erase the RSO if there is pointing drift. So, it is better to leave them. But they can be erased in the final image for cosmetic or human viewing purposes. A filter, similar to Eq. 60, can be used to declare explicitly the cosmic-ray hits when a pixel is brighter than the expected value (plus the tolerance variation). Eq. 62 can be rewritten for CR detection, i.e.;

$$\text{If } [(I^{-D}_{k}(i,j) - I^{med}(i,j)) > h_t] \; ; \text{ this is a cosmic-ray.} \tag{72}$$

In such a case, the cosmic ray can be erased by replacing the pixel value by the most probable value given by the median filter;

$$I^{-D-C}_{k}(i,j) = I^{med}(i,j) \tag{73}$$

'I^{-D-C}' is read; the drift-compensated ('$-D$') and cosmic-ray-hit cleaned ('$-C$') image.

5.12   Detecting serendipitous RSOs.

The previous processing framework is designed for the detection of expected RSOs with the maximum possible sensitivity. The drawback of the method is that it does not have the capability of detecting unexpected RSOs, even bright ones. This is a shortfall of methods designed with a-priori knowledge such as matched filter and TRM acquisition.

For detection of serendipitous RSOs acquired in SSM (sidereal stare mode), it is recommended to use other detection techniques such as those described in Refs. 7 and 8. Basically, these methods detect candidates in individual frames and then look for objects that have coherent alignment in the image sequence. Obviously, only bright objects can be detected in each frame of the sequence and be noted. These methods are not as sensitive as the method presented in this document.

In TRM, when an unexpected RSO is present in the FOV, there are two possible cases. It may have a motion very close to the other expected object and it can be detected as a member of the group of RSOs (see Section 4.9). The other possibility is that it has a very different motion and appears like a streak in images. If the streak alignment is the same as the stars, it will be detected as a different star in each frame. The only way to detect it is to observe that there is an unidentified star in each frame and the position pattern is coherent in the image sequence. This would require ad-hoc algorithms which are not yet developed. If the alignment is different, it will be equivalent to a cosmic-ray hit (CR) in the individual frames. However, it creates a coherent aligned pattern in the non-realigned image sequence. Here is an algorithm framework that could detect bright serendipitous RSOs:

1-   detect and remove stars in each frame,

2-   sum all the image frames into a single global image,

3-   detect streak patterns (whose orientation is different than the stars) with Hough transform,

4-   look for chopped streaks.

This will detect all CRs and all bright serendipitous RSOs. The difference between these two groups of object is that CRs are single uniform streaks (with various lengths) while RSOs will appear as chopped streaks (several exposures with dead time between the exposures). The regular chopping can be used for RSO detection. This may be an interesting algorithmic framework to further develop.

6   Processing scheme for RSO detection

For the detection of satellites in TRM mode, the global processing scheme is presented in the following figures. This scheme is based on the image model developed in the previous chapters. It illustrates how algorithms are sequenced along with their dependencies. For detection in sidereal tracking mode, the processing methodology has already been published in Refs. 1 and 2.

In this processing, the image background is the first thing to be eliminated. Section 5.2 explained that it can be estimated by different methods. Once it is adequately estimated, it is subtracted from the image, producing a background-free image 'I^{-B}'.

The next step consists of detecting the stars. This uses the satellite pointing and attitude parameters (pointing coordinates, motion and camera rotation) for the estimation of the length and orientation of the star streaks in the image. This will produce the convolution kernel 'Z(P^A(t)|t,t+dt)' used by the iterative matched filter. If there are enough very bright stars, this method can be replaced by a faster algorithm (a basic threshold method and Hough transforms) but the matched filter method guarantees a maximum of detected stars. Once the stars are detected ('I^{+S}'), they are extracted and their centres of intensity are evaluated. Then, the list of star relative brightness and location 'S$_k$(n,i,j,a$_n$)' is built.

Before performing the RSO detection, it is preferable to remove the star streaks from the images. This makes the evaluation of the total RSO signal more accurate and also decreases the number of false alarms. The bright star streaks (and possibly every streak) are already detected ('I^{+S}'). Their binary extraction masks 'M^S_k' are also already created. They can be used to reset the streak to zero in the images ('I^{-S}'). Because of the detection method that compares every frame of the sequence for the detection of the static object, it is not certain that the star erasing is really required. Tests will have to be performed to determine if streak removal improves detection performance. On the contrary, if tests demonstrate that the star streak must be erased and that the 'reset' method is not accurate enough, Ref. 1 explains a more accurate method that removes stars without leaving artifacts. This method could be adapted for the current case but this is probably not necessary.

Once the stars are detected, the images can be calibrated astrometrically, i.e., by establishing the relation between the pixel coordinates and their equivalent sidereal (Ra, Dec) coordinates. The star pixel locations are first corrected for the geometric distortion caused by the optics. Then, this information is compared with a star database, using commercial software (like 'PinPoint or 'TheSky'). This determines the relation '@$_k$' between the pixel indexes and sidereal coordinates. This calibration also determines the exact telescope pointing direction ray 'P^A(t)'. This also facilitates the evaluation of pointing errors and drifts.

Once the drift is known, the image frames 'I^{-S}' are re-aligned 'I^{-D}' and the RSO appears at exactly the same place in every frame. This allows the summation of all images 'I$^\Sigma$', which improves the SNR and increases global detection sensitivity. Sensitivity can also be increased by integrating the RSO signal over the PSF area 'I$^{\Sigma\,PSF}$' and/or using the nearest maxima 'I$^{-D}_k{}^{max}$'. Finally, the RSO detection 'Δ_{ij}' is performed with the double threshold test: 1) the global detection with the high threshold value and 2) the product of all individual detections with the lower threshold value.

Where an RSO is detected, the brightness is evaluated and the brightness constancy is verified. If the brightness suddenly increases for an individual frame, there is a high probability that this detection is corrupted by a CR or a star streak. The detection with the CR contamination can be ignored in the detection report, or, at least, in the brightness estimation. The star streak proximity can also be checked with the realigned streak mask 'M^{S-D}_k'.

When detection occurs, it must be reported. However, the pixel indices need to be rewritten in the original frame coordinates by cancelling the image realignment offset. The cumulative drift, which was subtracted from the image coordinates, must now be reintroduced in the detection coordinates. Afterward the geometric correction 'Ω^{-1}' must be applied to these coordinates. Finally, it remains only to apply the astrometric conversion '$@_k^{-1}$' to obtain the real RSO coordinates.

Tasking and acquisition (see Fig. 1)

Input data

I^0_k : Image sequence (t_k)

Pointing metadata $P^0(t_k)$, $Rot(t_k)$

Star database

Expected satellite positions $R^P(TLE, t_k)$

(A)　(B)　(C)

Background estimation:
I^{med} = smooth (median (I^0_1, I^0_2, … I^0_K))
$\langle B_k \rangle$ = min (I^{med} , $I^{med} \otimes$ Large PSF)

Streak pattern estimation:
$Z(P^A(t)|t,t+dt) =$
$f(P^0(t_k), Rot(t_k) | t_k, t_k+t)$

Background removal:
$I^{-B}_k = I^0_k - \langle B_k \rangle$

Streak detector:
iterative matched filter;
$\Lambda_{km} = I^{-B}_{km} \otimes Z(P^A(t)|t,t+dt)$
$I^{-B}_{k(m+1)} = \min\{I^{-B}_{km},\ 2\ \Lambda_{km}\}$

Streak extraction mask:
$M^S_k = \Lambda_k > \sigma_n$

Processing

Streak removal:
$I^{-S}_k = I^{-B} (1 - M^S_k)$

Mask segmentation;
$M^S_k = \Sigma M^S_{kn}$,
M^S_{kn}: individual streak

(D)

Individual streak extraction:
$I^{+S}_{kn} = M^S_{kn} * I^{-B}$

Star localization and brightness:
$S_k(n,i,j,a_n)$;
(i,j) = center of mass $\{ I^{+S}_{kn} \}$
a_n = total intensity $\{ I^{+S}_{kn} \}$

(E)

Figure 4: Processing scheme for the detection of RSO acquire in TRM mode

E

Geometric correction
$(i',j') = \Omega^{-1}(i,j);$
$S_k(n,i',j',a_n)$

A   B

Astrometry software

1- Star identification
$S_k(n,Ra,Dec) \leftarrow S_k(n,i',j',a_n)$

2- Calculation of astrometric
transformation parameters:
$(i',j')_k = @_k(Ra,Dec)$
$P^A(t_k)$: real pointing
$Rot^A(t_k)$: real camera rotation

C

Drift estimation;
$D(t_k) = d\,(P^A(t_k) - R^P(TLE,t_k)\,)\,/dt$
$D_k = \Omega\,(@_k(P^A(t_k) + D(t_k)\,)) - (i_0,j_0)$
Cumulative drift;
$$X_k = \sum_1^k D_k \ , \ 1 \le k \le K$$

D

Image alignment
(drift compensation);
$I^{-D}_k = I^{-S}_k\,(i - X_{ik}, j - X_{jk})$

Image summation;
$$I = \sum_{k-1}^{K} I^{-D}_k$$

F
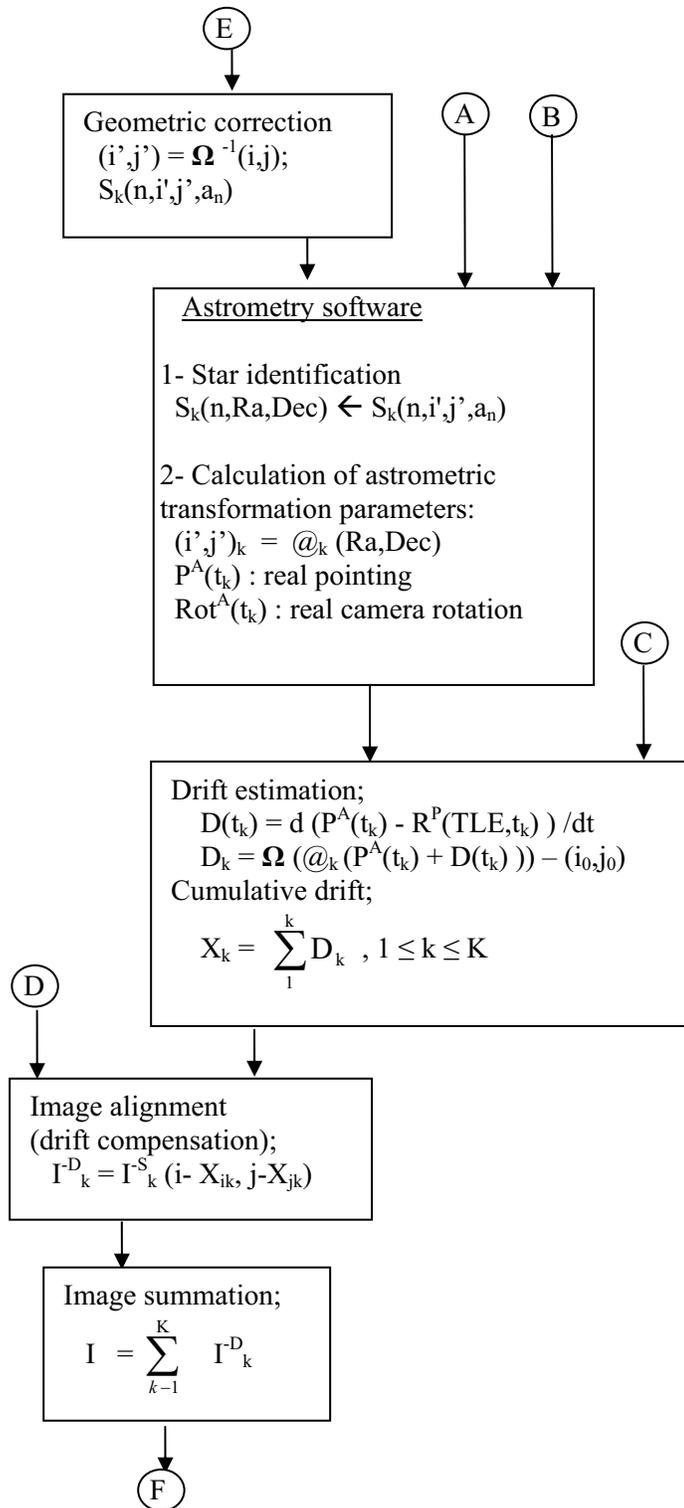
Figure 5: Processing scheme for the detection of RSO acquire in TRM mode:
continued from Fig 4

Option: Elimination of total residue;
$\langle B_\Sigma \rangle = I^\Sigma \otimes$ 'large impulse response',
$I^{\Sigma'} = I^\Sigma - \langle B_\Sigma \rangle$

(F)

(D)

Option: PSF integration;

$$I^{-D\,PSF}_k(i,j) = 1/(2n+1)^2 \sum_{i-n}^{i+n} \sum_{j-n}^{j+n} I^{-D}_k(i,j)$$

$$I^{\Sigma-PSF}(i,j) = 1/(2n+1)^2 \sum_{i-n}^{i+n} \sum_{j-n}^{j+n} I^\Sigma(i,j)$$

Option: Use local maxima;
$I^{-D\,max}_k(i,j) = \max(I^{-D}_k(i-n:i+n, j-n:j+n)$

(F)

RSO detection;
$\Delta_{ij} = [\, I^\Sigma(i,j) \geq h_h \,]\ \ldots$

$\ldots$ and $[\, \prod_{k=1}^{K} (I^{-D}_k(i,j) \geq h_l) \,]$

RSO-intensity estimation;
$\langle I^{RSO}(i,j) \rangle = I^{-D\,med}(i,j)$

(D)

Verification of brightness constancy
(verification of corruption by cosmis-ray hits)

$$\prod_{k=1}^{K} [\, (I^{-D}_k(i,j) - \langle I^{RSO}(i,j) \rangle)\ < h_t \,]$$

For valid detections, calculate centroid position
$R^A_{kn}(i,j) = X_k + $ center of intensity (I^{-D}_{kn}),
and report real position;
$R^A_n(t_k) = @_k^{-1}(\, \Omega^{-1}(R^A_{kn}(i,j))\,)$
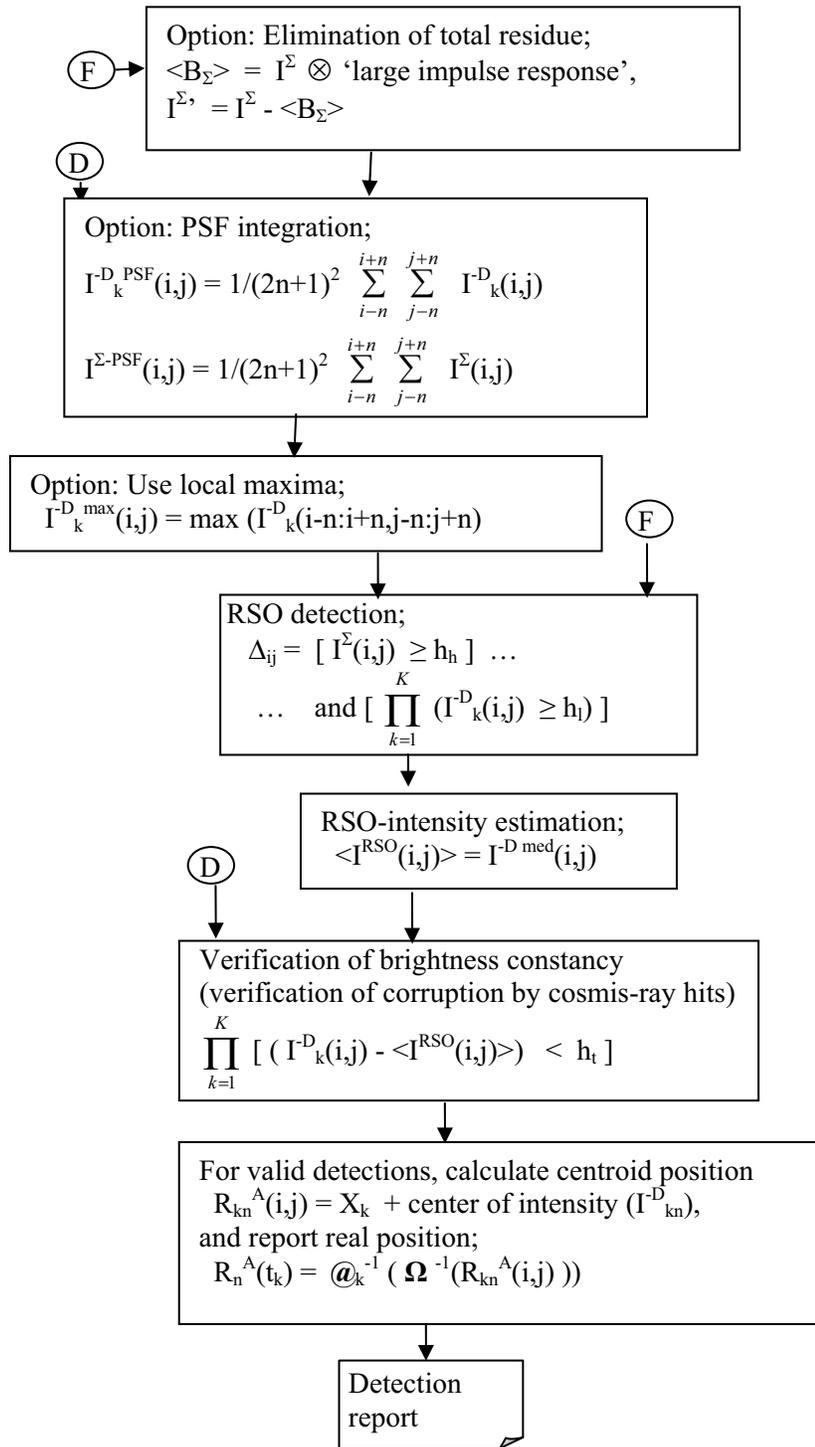
Detection
report

Figure 6: Processing scheme for the detection of RSO acquire in TRM mode:
continued from Fig 5

7 Conclusion

The strong expertise acquired with the past development of RSO detection algorithms (Refs. 1 to 4) allows the design of these algorithms which are specifically adapted for the detection in satellite tracking mode. These algorithms have not yet been fully coded nor tested, but the most challenging components have already been tested in previous works (Refs. 1 and 2). They are the iterative matched filter, the background and star removal methods, the astrometric calibration, image masking and segmentation, etc. All these algorithms are recycled and rearranged for the current case. This new method takes advantage of an acquisition method that acquires an image sequence, rather than a single one, which makes detection easier, more sensitive and more reliable. This introduces the need to measure the drift and realign the image, but this does not represent a difficult technical challenge.

This document will be used to guide the software development that will be required by space-based systems under development like NEOSSat or SAPPHIRE. Some algorithms may be changed for various reasons (performance, accuracy, fewer processing artifacts, sensitivity, etc), but the global approach should remain similar. Tests will have to be performed to fine tune the threshold values, for the evaluation of the detection sensitivity and for the drawing of the probability of detection graphs. All these tests will have to be performed with simulated data first because the real data may not be available at that time. The MOST satellite could provide similar real data, but this satellite was not conceived with a similar capability (like NEOSSat) for the acquisition of fast image sequences (short exposure and short download delay). Possibly, images from the MSX/SBV sensor (Space Based Visual) or the new SBSS (Space Based Surveillance of Space) satellite could be used for testing with real data if this data is made available to the developer team.

These algorithms were developed in the context of a space-based surveillance system but they can also be used by ground stations when they acquire images in TRM mode. The only characteristic of a space-based sensor is that it is exposed to cosmic rays and the images suffer from a source of noise that is not ordinarily present in a ground station data. On the other hand, data are not affected by the atmospheric transmission interferences, including turbulence. In TRM mode, both pointing systems are moving and only the final apparent RSO motion is taken into account; the fact that one sensor is moving while the other is at a fixed location is not an important parameter for image processing algorithms.

This method should be very sensitive. It is expected to be able to detect RSO as faint as SNR>3. It uses the fact that the fusion of the image sequence provides an improved SNR. At the same time, single detection, in the individual frames, can tolerate a very high rate of false alarms. The probability that there are false alarms at the same coordinates in every frame is almost null.

Contrary to popular opinion, cosmic-ray hits (CR) do not have to be erased in the images. Usually, the first processing step is a voting system in whuch the flashes cause by CRs are detected and erased. In TRM mode, this technique would affect the star streaks, which have the same behavior as the CRs. With current detection algorithms, CRs are ignored; when a CR trigs an alarm, it is detected in a single frame, not the whole sequence. In addition, a real detection can be corrupted, in one or several frames, by CRs or star streaks. However, when a possible detection is notified, brightness regularity is verified and the frames whose brightness suddenly becomes excessively hight are ignored. The keys for such detection performance are: the number of images in the sequence and the ability to realign the image which compensates for the RSO

drift. This drift compensation is possible because of the astrometric calibration and the knowledge about the prediction of the RSO position.

This processing scheme is not intended for on-board real-time processing; it requires too much processing capability. It is designed for post-acquisition processing by ground stations where all the required computing resources are available. Thus, in the intended mode of operations, imaging data are downloaded and updated RSO orbital parameters calculated on the ground. This greatly reduces risks for algorithm implementation as revisions (if necessary) can be readily implemented (no remote software updates required). Also, it permits on-ground diagnostics for cases when an RSO is not detected or ambiguous detection results occur.

References

[1] Lévesque M. P., Buteau S. 2007. Image processing technique for automatic detection of satellite streaks. DRDC Valcartier TR 2005-386. Defence R&D Canada - Valcartier.

[2] Lévesque M. P., Lelievre M., 2008. Improving satellite-streak detection by the use of false alarm rejection algorithms. DRDC Valcartier TR 2006-587. Defence R&D Canada – Valcartier.

[3] Lévesque M. P., Lelievre M., 2007. Evaluation of the accuracy of the dark frame subtraction method in CCD image processing. DRDC Valcartier TR 2006-343. Defence R&D Canada – Valcartier.

[4] Lévesque M. P., Lelievre M., 2008. Evaluation of the iterative method for image background removal in astronomical images. DRDC Valcartier TN 2007-344. Defence R&D Canada – Valcartier.

[5] 'http://www.bisque.com/Products/CCDSoft/' ', last access: Oct. 8th 2008.

[6] 'http://pinpoint.dc3.com/', last access: Oct. 8th 2008.

[7] Gural P.S., 'Matched filter processing for asteroid detection', The astronomical journal, 2005, pp.1951-1960.

[8] Toshifumi Y. Hirohisa K. and Atsushi N,. 'Activities of JAXA's innovative technology center on space debris observation, AMOS 2009, pp.777-806

List of symbols/abbreviations/acronyms/initialisms

CR	Cosmic-ray hit.
RSO:	Space Resident Object (satellite).
TLE:	'Two-Lines Element set': SSN's format for the parameters used to calculate the orbital position of a satellite.
SSN:	Space Surveillance Network.
FOV:	Field of view.
PSF:	Point Spread Function, which is also the optical impulse response.

General:

T:	Temperature.
t:	Time.
t (or dt):	Exposition time.
$\otimes$	Convolution operator.
Rot(t):	Rotation of the sensor at time 't'.

Coordinates systems:

$(i,j)_k$:	pixel index (i,j) of image frame 'k'.
(Ra,Dec,t):	(Right ascension, Declination, time).
k (lower case):	Frame index
K (upper case):	Number of frames in the image sequence.

Coordinate transformations:

$@_k$:	Coordinate transformation; $(i'',j'') = @_k(Ra,Dec)$
$\boldsymbol{\Omega}$:	Geometric distortion (optical distortion); $I^A_k (i',j') = I^A_k \, \boldsymbol{\Omega} \, (i',j')$
Θ:	Optical PSF; $I^A_k (i,j) = \Theta (I^A_k (i',j'))$

Scene elements:

A_k;	Astronomical scene.
a_n:	Intensity of the nth star.
$(Ra,Dec)_n$:	Location of the nth star.
a_R: Intensity of the RSO.	
$(Ra,Dec)_R^A$:	Location of the RSO.

$Z(P^A(t)|t,t+dt)$:   Streak shape produced by the pointing motion $P^A(t)$ during the time interval $t,t+dt$.

$Z((R^A(t)-P^A(t))|t,t+dt)$ Streak shape produced by the drift.

Position and pointing:

$\mathbf{R}^P(TLE,t) = (Ra, Dec, t)_R{}^P$:   Predicted position of the satellite.

$\mathbf{R}^A(t)$ $= (Ra, Dec, t)_R{}^A$:   Real position of the satellite

$\mathbf{P}^0(t)$ $= (Ra, Dec, t)_R{}^P$:   Pointing vector, determined with the onboard instruments.

$\mathbf{P}^A(t)$ $= (Ra, Dec, t)_P{}^A$:   Real pointing vector, determined with astrometry.

$\mathbf{D}(t)$:   Drift between two consecutive image frames.

$\mathbf{F}^P(t)$:   Pointing offset.

$\mathbf{F}^R(t)$:   RSO position offset.

Images components:

I^A: Image component containing only the stars.

I^R: Image component containing only the RSO.

I^0:   Original (acquired) image.

I^{-B}:   Background-free image.

I^{+S}:   Image component containing only the star streaks.

$I^{+S}{}_{kn}$:   A sub-image containing only the nth streak of the kth image frame.

I^{-S}:   Image frame where star streaks (and also the background) are removed.

I^{-D}:   Image frame where the drift is compensated (image realigned).

I^{Σ}:   Summation of the realigned image sequence.

B: Image background.

$<B>$:   Estimated image background.

$\mathcal{R}$:   Background residue (after background subtraction).

n: noise

σ_n: noise standard deviation.

$C_k(t)$:   Image component containing the cosmic-ray hits acquired during the exposure time.

Λ_k: Convolved image; the convolution peaks indicate the streak locations.

$\mathcal{D}$:   Dark frame.

$L_1(P^A(t_k), t)$:　　　　　　　　Astronomical scene background (zodiacal light, diffuse nebulae, etc.).

$L_2(P^A(t_k), t)$:　　　　　　　　Image background component caused by stray light.

M^S:　　　　　　　　　　　　Binary segmented mask image used to extract streaks.

S_{k-n}:　　　　　　　　　　　Sub-image containing only one streak.

$S_k(n,i,j)$:　　　　　　　　　List of the 'n' star centroid coordinates (i,j).

Detection:

h_h:　　　　　　　　　　　　High level detection threshold; for global detection.

h_l:　　　　　　　　　　　　Low level detection threshold; for detection in individual frame.

h_t:　　　　　　　　　　　　Brightness tolerance threshold; for cosmic-ray hit detection.

Δ_{ijk}　　　　　　　　　　　Detection at coordinates (i,j) in the frame 'k'.

$<I^{RSO}>$　　　　　　　　　　Once detected, estimation of the RSO brightness.

DOCUMENT CONTROL DATA

(Security classification of title, body of abstract and indexing annotation must be entered when the overall document is classified)

1. ORIGINATOR (The name and address of the organization preparing the document. Organizations for whom the document was prepared, e.g. Centre sponsoring a contractor's report, or tasking agency, are entered in section 8.) Defence R&D Canada –Valcartier 2459 Bould Pie XI north, Québec, QC, G3J 1X5.	2. SECURITY CLASSIFICATION (Overall security classification of the document including special warning terms if applicable.) UNCLASSIFIED

3. TITLE (The complete document title as indicated on the title page. Its classification should be indicated by the appropriate abbreviation (S, C or U) in parentheses after the title.) Image and processing models for satellite detection in images acquired by Space-based Surveillance-of-Space sensors   (U)

4. AUTHORS (last name, followed by initials – ranks, titles, etc. not to be used) Martin P. Lévesque

5. DATE OF PUBLICATION (Month and year of publication of document.) September 2009	6a. NO. OF PAGES (Total containing information, including Annexes, Appendices, etc.) 38	6b. NO. OF REFS (Total cited in document.) 8

7. DESCRIPTIVE NOTES (The category of the document, e.g. technical report, technical note or memorandum. If appropriate, enter the type of report, e.g. interim, progress, summary, annual or final. Give the inclusive dates when a specific reporting period is covered.) Technical Report

8. SPONSORING ACTIVITY (The name of the department project office or laboratory sponsoring the research and development – include address.) Defence R&D Canada –Valcartier 2459 Bould Pie XI north, Québec, QC, G3J 1X5.

9a. PROJECT OR GRANT NO. (If appropriate, the applicable research and development project or grant number under which the document was written. Please specify whether project or grant.)	9b. CONTRACT NO. (If appropriate, the applicable number under which the document was written.)

10a. ORIGINATOR'S DOCUMENT NUMBER (The official document number by which the document is identified by the originating activity. This number must be unique to this document.) DRDC Valcartier TR 2009-095	10b. OTHER DOCUMENT NO(s). (Any other numbers which may be assigned this document either by the originator or by the sponsor.)

11. DOCUMENT AVAILABILITY (Any limitations on further dissemination of the document, other than those imposed by security classification.) Unlimited

12. DOCUMENT ANNOUNCEMENT (Any limitation to the bibliographic announcement of this document. This will normally correspond to the Document Availability (11). However, where further distribution (beyond the audience specified in (11) is possible, a wider announcement audience may be selected.)) Unlimited

13. ABSTRACT (A brief and factual summary of the document. It may also appear elsewhere in the body of the document itself. It is highly desirable that the abstract of classified documents be unclassified. Each paragraph of the abstract shall begin with an indication of the security classification of the information in the paragraph (unless the document itself is unclassified) represented as (S), (C), (R), or (U). It is not necessary to include here abstracts in both official languages unless the text is bilingual.)

In the context of the surveillance of space, known resident space objects (RSO), i.e. active satellites and space debris, need to be acquired periodically to ensure that the knowledge of their orbital parameters is up-to-date. The most sensitive observation method consists of acquiring an image sequence while the target is actively tracked by the optical system such the RSO appears stationary in the image sequence. This generates an incredible amount of data which requires efficient detection algorithms and automated processing software. In this context, this document presents models for image formation, acquisition, and processing. From the observation request to the production of the images, the stream of events is briefly modeled. This ensures that a-priori knowledge and strategy will be applied to efficiently process the acquired data. These models produce a series of algorithms used to separate the image components and detect the RSO. This document presents algorithm diagrams that can be used to develop the processing software.

Dans le cadre de la surveillance de l'espace, les objets spatiaux connus en orbite (OSO), i.e., satellites actifs ou débris spatiaux, ont besoin d'être acquis périodiquement pour s'assurer que la connaissance de leurs paramètres orbitaux soit maintenu à jour. La méthode d'observation la plus sensible consiste à acquérir une séquence d'images lorsque la cible est poursuivie activement par le système optique et que l'OSO apparaît stationnaire dans la séquence d'images. Cela génère une quantité incroyable de données qui requièrent des algorithmes de détection efficaces et des logiciels de traitement automatisé. Dans ce contexte, ce document présente des modèles pour la formation, l'acquisition et le traitement des images. De la requête d'observation à la production des images, la chaîne des événements est modélisée brièvement. Cela permet de voir les connaissances et stratégies a priori qui peuvent être utilisées pour traiter efficacement le données acquises. Ces modèles produisent une série d'algorithmes utilisés pour séparer les composantes de l'image et détecter l'OSO. Ce document présente les diagrammes d'algorithmes qui seront utilisés pour développer le logiciel de traitement.

14. KEYWORDS, DESCRIPTORS or IDENTIFIERS (Technically meaningful terms or short phrases that characterize a document and could be helpful in cataloguing the document. They should be selected so that no security classification is required. Identifiers, such as equipment model designation, trade name, military project code name, geographic location may also be included. If possible keywords should be selected from a published thesaurus, e.g. Thesaurus of Engineering and Scientific Terms (TEST) and that thesaurus identified. If it is not possible to select indexing terms which are Unclassified, the classification of each should be indicated as with the title.)

Acquisition model, image model, satellite, detection, streak, matched filter, image background, drift, space-based sensor, TLE, algorithms, image processing, astrometry, tracking mode.

Defence R&D Canada

Canada's Leader in Defence
and National Security
Science and Technology

R & D pour la défense Canada

Chef de file au Canada en matière
de science et de technologie pour
la défense et la sécurité nationale

DEFENCE **R&D** DÉFENSE

www.drdc-rddc.gc.ca